Scripta Materialia xxx (2015) xxx–xxx

Contents lists available at ScienceDirect

Scripta Materialia

journal homepage: www.elsevier.com/locate/scriptamat

Glancing angle XRD analysis of particle stability under self-ion irradiation in oxide dispersion strengthened alloys

A.J. London [a,*], B.K. Panigrahi [b], C.C. Tang [c], C. Murray [c], C.R.M. Grovenor [a]

[a] Department of Materials, University of Oxford, 16 Parks Road, OX1 3PH, UK
[b] Materials Science Group, Indira Gandhi Centre for Atomic Research, Kalpakkam 603102, India
[c] Diamond Light Source, Harwell Science and Innovation Campus, Didcot, Oxfordshire OX11 0DE, UK

ARTICLE INFO

Article history:
Received 8 May 2015
Revised 24 July 2015
Accepted 27 July 2015
Available online xxxx

Keywords:
Oxide dispersion strengthened steel
ODS
Glancing incidence X-ray diffraction
Ion irradiation

ABSTRACT

We have used glancing-incident angle X-ray diffraction (GIXRD) to study the stability of oxide nanoclusters in an Fe–14Cr–0.2Ti–0.3Y_2O_3 ODS alloy. High dose self-ion irradiation produces damaged layers a few hundred nanometres deep normally requiring time-consuming, site-specific techniques to study them. We have shown that GIXRD provides an effective way to study the damage depth profile by varying the incident angle, and that the $Y_2Ti_2O_7$ nanoclusters in these alloys are disrupted by high dose irradiation at temperatures from 150 to 973 K.

Oxide dispersion strengthened (ODS) steels have been identified as a promising candidate structural material for possible Generation IV and fusion reactors because of their excellent high-temperature mechanical properties and improved radiation resistance when compared to conventional ferrite/martensite steels [1–3]. Additionally, they may also be useful as radiation-tolerant fuel cladding materials [4]. These properties are achieved by introducing stable oxide dispersions into the ferritic matrix which act as pinning sites for dislocations and sinks for irradiation-induced point defects [5–7]. ODS alloys are typically synthesized by ball milling pre-alloyed powders (Fe, Ti and Cr for instance) with Y_2O_3 powder to intimately mix the components [8,9]. These mechanically alloyed powders are then consolidated by hot extrusion [10] or hot-isostatic pressing [11] during which Y–Ti oxide nanoclusters form [5,12–14]. These nanoclusters have been reported to have different crystal structures and stoichiometries; including orthorhombic Y_2TiO_5, cubic $Y_2Ti_2O_7$, rock-salt structure, orthorhombic $Y_2Ti_2O_6$ or amorphous, depending on the alloy content and processing methods [15–17]. For instance, high resolution transmission electron microscopy (HRTEM) studies on the commercial MA 957 ODS alloy suggested that most of the oxide clusters are structurally consistent with cubic $Y_2Ti_2O_7$ [18–21], but other authors have detected both cubic $Y_2Ti_2O_7$ and orthorhombic Y_2TiO_5 clusters [15,22]. Barnard et al. [23] performed DFT calculations to identify the possible candidate structures for the smallest Ti–Y–O nanoclusters in ferritic alloys, indicating that clusters with the $Y_2Ti_2O_7$ pyrochlore structure are more stable than clusters coherent with the Fe lattice.

The radiation stability of these materials is important for future use, and ion irradiation is commonly employed as an analogue for the neutron damage these materials would experience in service [24,25]. Understanding the stability of the oxide nanoclusters under irradiation is critical for their future deployment, and has been studied by several groups [26–28] showing that the average residual nanocluster size depends on both the irradiation dose and irradiation temperature. Ion irradiation is quick, cheap and does not produce radioactive material, but takes place at a much accelerated rate and only produces a shallow depth of damage. Therefore, the previous experiments rely on techniques like atom probe tomography or high-resolution TEM that probe very small volumes of material. The use of high-resolution synchrotron X-ray diffraction to identify the crystal structure of the predominant nanoclusters has also been reported [1] but only for bulk samples. In this paper we present a study of the effect of high dose self-ion implantation on oxide nanoclusters in ODS steel using glancing angle XRD (GIXRD) to analyse the distribution of diffracting particles through the damaged region as a function of implantation temperature.

The samples we have studied in this work are selected from a research project on the structure and properties of model ODS alloys. They have a composition of Fe–14Cr–0.03C–0.2Ti–0.3Y_2O_3

* Corresponding author.
E-mail address: andrew.london@materials.ox.ac.uk (A.J. London).

http://dx.doi.org/10.1016/j.scriptamat.2015.07.037
1359-6462/

(all wt%), and were prepared by mechanical alloying and hot extrusion. The initial microstructure of these alloys has been previously reported [29]. 12 mm diameter, 0.5 mm thick disks were cut from extruded bars and mechanically polished to a mirror finish prior to ion irradiation by Fe ions as detailed in Table 1. Samples were irradiated at IGCAR, Kalpakkam, with a dose rate of approximately 3×10^{-3} dpa/s (~1100 or 350 nA current for 5 MeV and 1.8 MeV ions respectively), with a temperature stability of ±2 K and in a vacuum better than 10^{-7} mbar to limit surface oxidation.

The GIXRD experiments were carried out on beamline I11 at Diamond Light Source using a synchrotron X-ray beam of $\lambda = 0.825650(10)$ Å ($E \sim 15$ keV). The wavelength was calibrated using a high quality silicon powder (SRM640c). This high brightness beamline is designed to perform high-resolution powder diffraction experiments [30] such as the detection of weak features in crystalline structures or low concentration components in complex phase mixtures. Since the instrumental contribution to the peak width is small (FWHM ~ 0.003° at $2\theta \leqslant 30°$), diffraction peak broadening comes mainly from size-strain effects in the sample [30]. Recently, a new alignment stage has been added to the diffraction instrument for GIXRD. With precise control of the angle between the incident X-ray beam and sample surface, the penetration depth of the incident X-rays into the surface is controllable. The alignment stage also improves the signal/background contrast, which is particularly beneficial for studying changes in phase distributions just below the sample surface (~nm–μm) caused by specific treatments or processing. Using a beam size of 0.15 (vertical) × 2.5 mm (horizontal), an illuminated footprint of a few mm^2 was achieved for each measurement. As damage of ODS alloys by self-ion irradiation is predominantly a surface effect, the apparatus was used to probe the stability of oxide nanoclusters in the ODS materials described above. We used incident angles of 0.25°, 1°, 2° and 4°, resulting in calculated attenuation depths of 45, 400, 800 and 1610 nm respectively. These X-ray $1/e$ attenuation depths were calculated as a function of glancing incidence angle into a $Fe_{88}Cr_{12}$ alloy with a 15 keV beam energy using the method detailed in [31]. The irradiation damage profile was calculated using the Stopping and Range of Ions in Mater (SRIM) [32] software. This allows us to estimate whether we are probing diffraction information from above, in or below the peak damage region. SRIM calculations were performed using the simple damage calculation, 40 eV displacement energy and zero lattice binding energy [32].

Fig. 1 shows a typical powder diffraction two-theta scan from unirradiated material with a glancing angle of 4°. Peaks in the GIXRD data were identified as reflections from the ferritic FeCr matrix, mixed Fe–Cr surface oxides, Cr_2O_3, $M_{23}C_6$ carbides and from the cubic $Y_2Ti_2O_7$ phase [1]. The region around the $Y_2Ti_2O_7$ (222) peak is shown in detail in Fig. 2a; this peak is used to monitor the behaviour of the nanoclusters. There was no sign in any diffractogram of the strongest peaks from the Y_2TiO_5 phase, (203) and (210), which should appear at 15.6° and 15.8° 2θ respectively. Fig. 2 compares data from the as-received condition and after the ion-irradiations defined in Table 1. With an incident

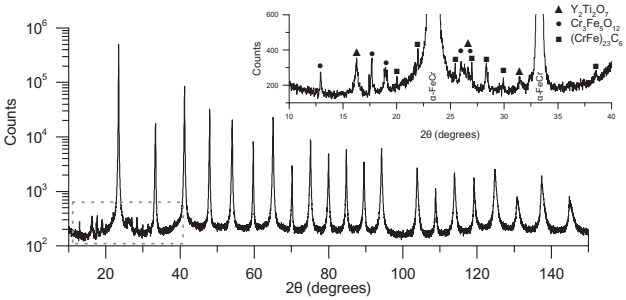

Fig. 1. Typical GIXRD pattern from a Fe–14Cr ODS alloy, $\lambda = 0.825650(10)$ Å, showing the main ferritic peaks. The inset shows reflections indexed as the Y–Ti nano-oxide particles, surface oxide and Fe–Cr carbide.

angle of 2° in Fig. 2b we are probing mostly material which has seen a high ion dose. The $Y_2Ti_2O_7$ (222) integrated peak intensities in the samples implanted at both 773 and 973 K are substantially reduced compared to the as-received sample, from 3100 to under 900 integrated counts in sample B for example. There was only a change in peak intensity and no significant change in peak width or position. This lower peak intensity suggests that the nanoclusters have a reduced volume fraction or are damaged, but not removed altogether as a result of irradiation at $T_{irrd} > 700$ K. This is consistent with previous reports which indicate that the nanoclusters persist (or are dynamically reformed) after irradiation at higher temperatures [26]. Samples B and C ($T_{irrd} = 773$ and 973 K) showed similar $Y_2Ti_2O_7$ (222) peak intensities, but sample C showed an increased intensity in carbide peaks suggesting significant coarsening of $M_{23}C_6$. By contrast, the data from the sample irradiated at 150 K in Fig. 2a shows that the $Y_2Ti_2O_7$ (222) peak has been almost completely lost. Peaks from $M_{23}C_6$ where not visible in sample A.

Fig. 3c shows in more detail the influence of irradiation at 150 K on the distribution of particles contributing to the $Y_2Ti_2O_7$ (222) reflection by using glancing incidence angles from 0.25° to 4°. By varying this angle, we are probing depths from the near-surface region to below the predicted range of the implantation damage (0.9 μm, see the SRIM profile in Fig. 3a). Peak intensities have been calculated by a simple background subtraction routine that generates integrated counts for each (222) peak from each full two-theta scan at each incident angle. The fitted curves, including the background, are shown as solid lines in Fig. 2. For the as-received material, the peak steadily increases in intensity with angle because a larger volume of material is contributing to the diffracted intensity, but this increase is not seen in the data from sample A. From A, up to an attenuation depth of 500 nm (1.25°), no diffracted intensity was observed, presumably as a result of dissolution, amorphisation or significant refinement of the $Y_2Ti_2O_7$ nanoclusters in the damaged region. At higher angles, the peak intensity in sample A increases as the undamaged region below the implantation range is probed at greater incident angles. The depth of the region of reduced (222) intensity relative to the reference sample corresponds well with the predicted damage range due to the Fe^+ ion irradiation calculated using SRIM [32]. To confirm that we are interpreting this change in diffracted intensity correctly, Fig. 3b shows the 3D positions of yttrium, titanium and oxygen containing species (black points) as analysed by atom probe tomography from an approximate sample depth of 350–850 nm in sample A. This data indicates that the nanoclusters are severely disrupted near the peak of the damage profile to 100 dpa, in agreement with other recent studies [27,33] which show the nanoclusters can be dissolved by ion irradiation at cryogenic temperatures.

Table 1
Details of the ion irradiation conditions for samples A–C.

Sample	A	B	C
Irradiation temperature (K)	150	773	973
Ion & energy (MeV)	Fe^+	Fe^{3+}	Fe^{3+}
	1.8	5.0	5.0
Dose (10^{16} ions/cm^2)	4.5	15	15
Peak damage (dpa)	100	150	150
Total damage depth (um)	0.9	1.9	1.9